Article:
Paulose Nadappuram, B, Cadinu, P, Barik, A et al. (12 more authors) (2019) Nanoscale Tweezers for Single Cell Biopsies. Nature Nanotechnology, 14. pp. 80-88. ISSN 1748-3387

https://doi.org/10.1038/s41565-018-0315-8

Nanoscale Tweezers for Single Cell Biopsies

Binoy Paulose Nadappuram,[1, †] Paolo Cadinu,[1, †] Avijit Barik,[2] Alexander J. Ainscough,[1,3] Michael J. Devine,[4] Minkyung Kang,[1] Jorge Gonzalez-Garcia,[1] Josef T. Kittler,[4] Keith R. Willison,[1] Ramon Vilar,[1] Paolo Actis,[5] Beata Wojciak-Stothard,[3] Sang-Hyun Oh,[2] Aleksandar P. Ivanov,[1, *] and Joshua B. Edel[1, *]

[1] Department of Chemistry, Imperial College London, SW7 2AZ, UK.
[2] Department of Electrical and Computer Engineering, University of Minnesota, Minneapolis, Minnesota, 55455, USA.
[3] Department of Experimental Medicine and Toxicology, Imperial College London, W12 0NN, UK.
[4]Department of Neuroscience, Physiology and Pharmacology, University College London, London, WC1E 6BT, UK
[5] School of Electronic and Electrical Engineering, Pollard Institute, University of Leeds, LS2 9JT, UK

[†] Authors contributed equally
[*] Corresponding authors: joshua.edel@imperial.ac.uk, alex.ivanov@imperial.ac.uk

Abstract

Much of the functionality of multi-cellular systems arises from the spatial organisation and dynamic behaviours within and between cells. Current single-cell genomic methods only provide a transcriptional "snapshot" of individual cells. The real-time analysis and perturbation of living cells would generate a step-change in single-cell analysis. Here we describe minimally invasive nanotweezers that can be spatially controlled to extract samples from living cells with single-molecule precision. They consist of two closely spaced electrodes with gaps as small as 10-20 nm, which can be used for the dielectrophoretic trapping of DNA and proteins. Aside from trapping single molecules, we also extract nucleic acids for gene expression analysis from living cells, without affecting their viability. Finally, we report on the trapping, and extraction of a single mitochondrion. This work bridges the gap between single-molecule/organelle manipulation and cell biology and can ultimately enable a better understanding of living cells.

Introduction

Understanding the molecular diversity of seemingly identical cells is crucial in elucidating the genetic heterogeneity of tissues and organs to aid the accurate design of disease models and patient-specific therapies[1-4]. The key enabling technologies for single-cell genomics have emerged from the convergence of advanced engineering with molecular and cellular biology[5,6]. Examples include microfluidic 'lab-on-a-chip' platforms incorporating single-cell manipulation techniques such as microwell-based docking[7-10], electrokinetic single-cell focusing[11], fluorescence activated cell sorting[12, 13] and optical tweezers[14-16]. There is now a thriving community of researchers applying single-cell technologies to deliver insights into applications such as clonal evolution in cancer[17] and somatic variations acquired in normal tissue throughout life[18, 19], novel cell types and states in multi-cellular organisms[20, 21] and the heterogeneity of bacterial populations[22]. These methods now underpin one of the most ambitious genomics projects after the sequencing of the human genome, the "Human Cell Atlas" which aims to create a reference map of all human cells[23]. However, these methods require the removal of the target cell from its microenvironment, leading to loss of interconnection and in most cases, its lysis. This limitation negates the ability to perform dynamic studies as the output is simply a "snapshot" of the cell transcriptional profile at a particular point in time.

To circumvent this problem, a number of techniques have been developed to enable dynamic studies of single living cells[24, 25]. For example, the insertion of non-destructive sampling devices based on atomic force microscopy (AFM)[26, 27] and nanopipettes[28-30] allowed for the extraction of nucleic acids from individual cells. Furthermore, the functionalization of AFM tips with nucleic acid probes enabled the analyses of specific gene expression in living cells[31-34]. A method employing fluid force microscopy extended the use of AFM tips to intracellular fluid extraction for single-cell analysis[24]. Nevertheless, both fluid force microscopy and nanopipette based extraction strategies involve the non-specific aspiration of cytoplasmic fluid, which compromises cell viability.

We report on the development of minimally invasive nanotweezers that can be spatially controlled to extract molecular samples from individual living cells with single-molecule precision. This biopsy method does not aspirate cytoplasmic fluid and allows for the preconcentration of analyte in real time. This is a particularly powerful technique especially for the detection of molecular species present in low copy numbers, which are currently elusive to state-of-the-art methods. These nanotweezers utilise dielectrophoresis (DEP) to trap molecules subjected to a non-uniform electric field and are composed of two individually addressable nanoelectrodes separated by a ~10-20 nm insulating septum. High electric field gradients ($\nabla|E|^2 \sim 10^{28}\ V^2m^{-3}$) are generated enabling the trapping of single molecules at physiological ionic strengths. The capabilities of the technique were validated by performing trapping and extraction of small protein molecules (<15 kDa) and single DNA molecules from aqueous solutions. Further, we demonstrate the suitability of the nanotweezers for use in single-cell biopsies to extract DNA directly from the nucleus of human osteosarcoma (U2OS) cells and primary human pulmonary artery endothelial cells (HPAEC). Similarly, RNA was extracted by sampling the cytoplasm of the HPAECs for genomic analysis, Fig. 1a. We also show that the nanotweezer can be used to perform single organelle manipulation by trapping and extracting single mitochondrion from primary rodent hippocampal neurons in culture. Being fully compatible with scanning probe microscopy these dielectrophoretic probes can ultimately provide the basis of multiple time point and spatial sampling of the same cell or tissues for genomic, gene expression and single organelle analysis.

Results and Discussion

The nanotweezers described herein were fabricated using nanopipettes made from double-barrelled quartz theta capillaries via laser pulling[35, 36]. Two coplanar carbon electrodes were formed at the tip of the nanopipette by pyrolytic deposition of carbon[37-39]. The carbon deposition was achieved by filling the nanopipette barrels with butane under an argon atmosphere (Supplementary Information,

section 1). Field-emission scanning electron microscopy (SEM) and transmission electron microscopy (TEM) images of a representative nanotweezer before and after carbon deposition are shown in Fig. 1b. The nanotweezer consists of two co-planar semi-elliptical nanoelectrodes with dimensions of the major and minor axes being 26 ± 11 nm and 23 ± 6 nm respectively (n=10). The two electrodes were separated by a quartz septum 10 – 20 nm in width (along the major axis). Elemental analysis of the fabricated nanotweezer (Supplementary Information, section 2) confirmed the presence of a continuous carbon filling inside the nanopipette. Each nanoelectrode was individually characterised using the steady-state current for the one-electron reduction of hexaamminerutheniumIII) chloride ($Ru(NH_3)_6Cl_3$) and followed a characteristic sigmoidal response, Fig. 1c and Supplementary Information, section 3. The electrode to electrode variation was within 6 nm as indicated by the variation in the magnitude of the limiting currents. DEP was generated by applying an *AC* signal to the nanoelectrodes via copper wires inserted through the back end of the nanopipette barrels.

The application of an AC field across the electrodes creates an electric field gradient, which can exert an attractive force (depending on the conductivity and dielectric permittivity between an electrically polarizable particle and its surrounding medium) on polarizable objects near this field. This force depends on the electric field gradient ($\nabla|E|^2$) and can be used to trap and manoeuvre particles. To trap and concentrate nanoscale entities such as biomolecules, DEP forces in the order of fN are required to overcome Brownian motion,[40] convective flow due to heating, and electrohydrodynamic effects[41]. Since $\nabla|E|^2$ is proportional to V^2L^{-3} (where V is the applied voltage and L is the distance between electrodes), larger trapping forces can be achieved either by increasing the voltage between the electrodes or by reducing the distance between them[42]. However, the application of a higher voltage can lead to unwanted heat generation, bubble formation, and electrochemical reactions and hence is not desirable for manipulating biomolecules inside or outside of living cells[42, 43].

In our case, the close spacing of the two coplanar carbon electrodes offered the possibility of generating high dielectrophoretic forces without employing high voltages. From finite element method (FEM) calculations, field gradients ($\nabla|E|^2$) as high as 10^{28} V^2m^{-3} near the electrode gap could be obtained (Fig. 1d (i)**,** Supplementary Information, section 4), which is significantly higher than previously reported for single-cell screening platforms based on DEP[34] and approximately two orders of magnitude higher than metal electrode based DEP systems[40, 42, 43]. With such high field gradients, single DNA molecules well below 200 bp, could be trapped, Fig. 1d (ii). A 2D plot of $\log_{10}(\nabla|E|^2)$ around the nanotweezer tip was constructed, to visualise the strength of the electric field intensity gradient and the trapping force. The projection of the field gradient along the z-axis (along the length of the nanopipette) revealed a highly localised trapping field at the tip. Hence, it was possible to operate the nanotweezer at voltages as low as V_{RMS}= 1 V (V_{pp}=3 V), to minimise effects associated with heating especially in higher conductivity solutions (e.g. cytoplasmic conductance of a human cell) as shown in Fig. 1e.

Single molecule trapping in solution

The effectiveness of the nanotweezer was experimentally validated by trapping and extracting fluorescently labelled DNA of different sizes (ranging from 22 base ssDNA to 48,502 bp dsDNA) and small proteins such as monomeric α-synuclein (14.5 kDa) (Supplementary Information, section 5-7). Visualisation of the trapping was achieved using a YOYO-1 labelled 100 pM 10 kbp dsDNA solution containing 1 mM KCl. To draw 10 kbp dsDNA towards the tip, a minimum trapping force of 9.92 fN is required[40], which correspond to a $|\nabla|E|^2|$ higher than 2.5 x 10^{16} V^2 m^{-3}, Fig 1d (ii). From FEM simulations, the DEP trapping volume extends to approximately 300 nm from the nanotweezer tip (Fig. 1d (ii) and S3) which is sufficient to trap the DNA efficiently. Application of an *AC* voltage at a frequency of 1 MHz and a peak-to-peak voltage of 20 V, resulted in the accumulation and concentration of DNA molecules at the nanotweezer tip, Fig. 2a and 2b. Levelling of the

fluorescence intensity was observed soon after the *AC* field was turned on and attributed to saturation of DNA accumulated at the tip. When the *AC* voltage was turned off, the fluorescent intensity decreased as the molecules freely diffused away from the tip. As a control in the absence of an *AC* voltage, no fluorescence was observed confirming minimal to no non-specific adsorption of DNA onto the carbon electrodes.

As expected, the trapping efficiency was directly dependent on applied peak-to-peak voltage (V_{pp}) and frequency (f_A), Figs. 2c and d. The fluorescence intensity and hence the number of molecules in the trap was found to increase with increasing f_A up to 1.5 MHz followed by a rapid decrease. The variation of the trapping efficiency with frequency can be attributed to the change in polarizability of DNA molecules at different *AC* fields, which arises from the variation in the relaxation time constant of the ions surrounding the DNA[42]. At higher frequencies, the counterions present in the solution do not have enough time to redistribute in each alternation of the *AC* voltage resulting in low polarizability. Since the DEP force on a DNA molecule is directly proportional to its polarizability ($\vec{F}_{DEP} = \frac{1}{4}\alpha\nabla|E|^2$, where α is the polarizability of the molecule) this leads to a low DEP force acting on the DNA molecule resulting in low trapping efficiency at higher frequencies[40].

Confirmation that the nanotweezer does not affect the functional integrity of the DNA was obtained by selective amplification of the DNA, extracted from solution by using quantitative polymerase chain reaction (qPCR). After holding the nanotweezer in solution for 30 seconds, it was gradually retracted, while the *AC* voltage was kept on. The extracted DNA was then transferred into qPCR tubes for amplification and melting curve analysis. Fig. 2e show representative amplification curves with a threshold cycle (C_t) value of 32 ± 2 corresponding to approximately 37 extracted DNA molecules. In comparison, a positive control obtained at a DNA concentration of 0.4 ng 10 kbp dsDNA produced a C_t = 12 ± 1 while no amplification was observed for the negative control whereby the nanotweezer was held in solution without applying an *AC* voltage (Supplementary Information, section 8). A melting peak at 84 °C was observed for both the samples and the positive control further confirming successful amplification. Similar experiments were also successfully performed with a solution of 10 pM λ-DNA (48.5 kbp), Supplementary Information, section 9.

By decreasing the DNA concentration down to 100 fM it was possible to optimise the trapping to selectively trap single molecules, Fig. 3. Time-dependent images along with pixel intensity profiles are shown at various stages of trapping and release process Fig. 3b and c (i-iv). Much like at higher concentrations, upon application of the *AC* field, the molecule is first pulled towards the nanotweezer tip. Once inside the trapping volume, the molecule stays there as long as the *AC* field is kept on. This was further demonstrated for three different nanotweezers using λ-DNA, Fig. 3d. Fluorescence intensity vs time traces are shown for two tips where a single molecule is trapped (i-ii) and another where three molecules are sequentially trapped (iii). Corresponding qPCR amplification curves confirmed nearly 100% amplification of the trapped molecules, Fig. 3e. Furthermore, sequencing confirmed that the amplified segment was >99% identical to the corresponding segment of λ-DNA, Fig. 3f. A unique feature of the nanotweezer is that it can be used in combination with an XYZ positioning platform to perform '*pick-and-place*' type measurements where single molecules can be trapped, moved at a velocity as high as 30 µm s^{-1} and then released. This was demonstrated for 10 kbp DNA, Fig. 3g and Supplementary Information, section 10 where a single molecule was traced using an image tracking algorithm to follow the trajectory of the molecule from capture (i), to movement in the x-y plane (ii-iii) and subsequent release (iv).

Molecular trapping inside of cells

Having established the capability of trapping and releasing single-molecules in solution, we used nanotweezers to perform highly localised single cell biopsies. In particular, we explored i) the possibility of targeting different compartments such as the nucleus and cytoplasm, ii) selective

sampling of cellular building blocks (e.g. DNA, RNA, and organelles) and iii) the versatility of using the extracted material in standard biomolecular assays. Human immortalised (U2OS) and primary (HPAEC) cells were utilised with the purpose of sampling genetic material from the nucleus (Fig. 4a-c). To visualise the extraction of DNA, U2OS cells were stained using a DNA binding dye (DAOTA-M2)[44]. Individual cells were approached using a micromanipulator and imaged using optical microscopy. The nanotweezers tip was inserted into the cell nucleus, and an *AC* bias applied (f_A = 1 MHz, V_{pp} = 20 V). Analogous to the solution-based extraction, DNA molecules and fluorescent beads were concentrated at the tip as can be seen by the localised increase in fluorescence (Fig. 4d-e, panels i and ii, Supplementary Information, section, 10). Based on numerical simulation and characterisation of the trapping stability (Supplementary Information, section, 11 & 12), it was reasonable to assume that the generated DEP force was sufficiently large to rupture part of a chromosome resulting in DNA fragments being captured around the tip. After being held inside the nucleus for the desired time (10 s), the nanotweezer tip was retracted from the cell with the *AC* voltage kept on, to complete the extraction. A fluorescent spot at the tip confirmed the successful extraction. The same procedure was followed for performing label-free single cell biopsies. DNA was sampled from the nucleus of unstained HPAEC cells and then subjected to qPCR amplification of a target sequence in 45S ribosomal DNA (rDNA). A part of the 45S rDNA sequence was amplified using a pair of specific primers along with *ACTB* DNA template as the positive control, Fig. 4f-g. A C_t value of 33 ± 1 confirmed the presence of 45s rDNA sequence on the extracted sample at the nanotweezer tip. It was highly likely that the extracted DNA contained at least one copy of 45S rDNA as they are present in human chromosomes 13, 14, 15, 21 and 22, with total diploid copy number ranging from 60 to >800 repeat units[45].

The ability to operate at the single molecule level was demonstrated by extracting individual mRNA molecules from the cytoplasm of HPAEC cells. Proto-Oncogene 1 Transcription Factor (*ETS-1)* mRNA was first fluorescently labelled using *in situ* hybridisation, Fig. 5a (i), then the nanotweezer was positioned adjacent to the selected mRNA (Fig 5a (ii)), which then captured (Fig 5a (iii)) and subsequently withdrawn from its original position (Fig. 5a (iv)). Also, the sampling of RNA material was repeated using a different cell-permeable dye (SYTO™ RNASelect™) which selectively binds to the RNA molecules inside the cytoplasm (Fig. 5b), and can be extracted as confirmed by the fluorescent spot at the end of the tip (iii).

Due to the small trapping volume of the nanotweezer, there is a low probability of trapping low copy number mRNAs inside the cell. This was verified by confirming the presence of two low copy number mRNAs (<100), *ETS-1* and Krüppel-like Factor-2 (*KLF-2*) and one high copy number (>1000) mRNA*,* beta-*actin* (*ACTB*). mRNAs in the extracted sample was reverse transcribed, and the subsequently obtained cDNA was then subjected to qPCR. A part of the sequence in the cDNA was amplified using a pair of primers specific to *ETS-1, KLF-2* and *ACTB* gene sequences. In the case of *ETS-1* and *KLF-2*, no amplification was observed. However, *ACTB* was successfully amplified as is shown in Fig. 5c-d. Omitting the biopsies without mRNA hits (~50%), an average C_t value of 35 ± 2 for the extracted samples was obtained corresponding to an initial copy number ranging between 45 and 179 *ACTB* cDNA molecules (Supplementary Information, section, 13). The possibility of performing multiple sample extractions at different time points from the same cell was also assessed. In this case, two biopsies were carried out one hour apart from each other in different cytoplasmic locations. The viability of the cell after the two biopsies was monitored for up to 16 hours (supplementary information, section 14) to rule out any significant cell membrane damage during/after the extraction process.

Finally, the nanotweezers were used to extract subcellular structures such as organelles. Single mitochondria were removed from the axons of primary mouse hippocampal neurons in culture (Fig. 6a, b). The force exerted by the nanotweezer was sufficient to trap and extract the mitochondrion from the neuron (Fig. 6c) as confirmed by the fluorescence signal decrease at the

extraction point (Fig. 6d). The viability of extracted mitochondria was validated by repeating these experiments with mitochondria labelled with tetramethylrhodamine methyl ester (TMRM), a dye that is readily sequestered by active mitochondria and reflects intact mitochondrial membrane potential. Fig. 6e shows the fluorescence-time trace recorded at the mitochondrion before, during and after the trapping. No significant loss in fluorescence was observed during the trapping and extraction of the mitochondrion, indicating the feasibility of using nanotweezers for single organelle transplantation.

Conclusions

We have demonstrated the fabrication and use of a nanopipette based DEP nanotweezer for highly localised and minimally invasive extraction of intracellular molecules with single-molecule resolution in physiological environments. These nanotweezers are simple and inexpensive to fabricate and are composed of two individually addressable nanoelectrodes separated by a nanoscale septum to generate ultra-high electric field gradients required for trapping and manipulation (extraction and release) of different single molecules. The nanotweezers have a minimal footprint which enables direct access to the cell nucleus or cytoplasm without affecting their viability.

We were able to perform extraction of nucleic acids and proteins from highly dilute solutions (down to 100 fM) while confirming the functional integrity of the extracted molecules and demonstrate precise 'pick-and-place' operation of single molecules/particle. The technology allowed us to trap and extract molecules as small as 22 bases ssDNA. Further, we successfully employed these nanotweezers to trap efficiently and extract with high spatial accuracy, DNA from the cell nucleus and RNA molecules from the cytoplasm, while preserving their functional integrity, from different types of live human cells for single-cell DNA analysis and RNA for single-cell gene expression analysis. Additionally, we also demonstrated the single organelle manipulation capability of the nanotweezers.

When used in conjunction with an appropriate positioning platform, these nanotweezers can be used to investigate localised gene expression by extracting mRNAs from the target sites in the cell or to track protein expression inside the cell in response to external stimuli (for example, drug/antigen). Moreover, these nanotweezers could be easily modified and integrated with other electrochemical scanning techniques such as scanning ion conductance microscopy (SICM) which would allow for spatial and temporal quantification of gene expression within a single cell.

References

1. Tseng, F.-G. & Santra, T. S. *Essentials of Single-cell Analysis: Concepts, Applications and Future Prospects*. (Springer, Berlin, 2016).
2. Borland, L. M., Kottegoda, S., Phillips, K. S. & Allbritton, N. L. Chemical analysis of single cells. *Annu. Rev. Anal. Chem.* **1,** 191-227 (2008).
3. Trouillon, R., Passarelli, M. K., Wang, J., Kurczy, M. E. & Ewing, A. G. Chemical analysis of single cells. *Anal. Chem*. **85**, 522-542 (2013).
4. Higgins, S. G. & Stevens, M. M. Extracting the contents of living cells. *Science* **356**, 379-380 (2017).
5. Gawad, C., Koh, W. & Quake, S. R. Single-cell genome sequencing: current state of the science. *Nat. Rev. Genet.* **17**, 175-188 (2016).
6. Blainey, P. C. & Quake, S. R. Dissecting genomic diversity, one cell at a time. *Nat. Methods* **11**, 19-21 (2014).
7. Park, M. C., Hur, M. C., Cho, H. S., Park, S. H. & Suh, K. Y. High-throughput single-cell quantification using simple microwell-based cell docking and programmable time-course live-cell imaging. *Lab Chip* **11**, 79-86 (2011).
8. Mu, X., Zheng, W. F., Sun, J. S., Zhang, W. & Jiang, X. Y. Microfluidics for manipulating cells. *Small* **9**, 9-21 (2013).

9. Wang, J., Trouillon, R., Dunevall, J. & Ewing, A. G. Spatial resolution of single-cell exocytosis by microwell-based individually addressable thin film ultramicroelectrode arrays. *Anal. Chem*. **86**, 4515-4520 (2014).
10. Kimmerling, R. J. et al. A microfluidic platform enabling single-cell RNA-seq of multigenerational lineages. *Nat. Commun*. **7**, 10220 (2016).
11. Gao, J., Riahi, R., Sin, M. L. Y., Zhang, S. F. & Wong, P. K. Electrokinetic focusing and separation of mammalian cells in conductive biological fluids. *Analyst* **137**, 5215-5221 (2012).
12. Fu, A. Y., Spence, C., Scherer, A., Arnold, F. H. & Quake, S. R. A microfabricated fluorescence-activated cell sorter. *Nat. Biotechnol.* **17**, 1109-1111 (1999).
13. Liu, L., Cheung, T. H., Charville, G. W. & Rando, T. A., Isolation of skeletal muscle stem cells by fluorescence-activated cell sorting. *Nat. Protoc*. **10**, 1612-1624 (2015).
14. Norregaard, K. et al. Manipulation and motion of organelles and single molecules in living cells. *Chem. Rev*. **117**, 4342-4375 (2017).
15. Zhang, H. & Liu, K. K. Optical tweezers for single cells. *J. R. Soc., Interface* **5,** 671-690 (2008).
16. Ashkin, A., Schütze, K., Dziedzic, J. M., Euteneuer, U. & Schliwa, M. Force generation of organelle transport measured in vivo by an infrared laser trap. *Nature.* **348**, 346-348 (1990).
17. Wang, Y. et al. Clonal Evolution in Breast cancer revealed by single nucleus genome sequencing. *Nature* **512**, 155-160 (2015).
18. McConnell, M. J. et al. Mosaic copy number variation in human neurons. *Science* **342**, 632-637 (2013).
19. Cai, X. et al. Single-cell, genome-wide sequencing identifies clonal somatic copy-number variation in the human brain. *Cell Rep.* **8**, 1280-1289 (2014).
20. Villani, A. C. et al. Single-cell RNA-seq reveals new types of human blood dendritic cells, monocytes, and progenitors. *Science* **356**, eaah4573, (2017).
21. Macaulay, I. C. et al. Single-cell RNA-sequencing reveals a continuous spectrum of differentiation in hematopoietic cells. *Cell Rep*. **14**, 966-977 (2016).
22. Lan, F., Demaree, B., Ahmed, N. & Abate, A. R. Single-cell genome sequencing at ultra-high-throughput with microfluidic droplet barcoding. *Nat. Biotechnol*. **35**, 640-646 (2017).
23. Regev, A. et al. The human cell atlas. *eLife* **6**, 27041 **(**2017).
24. Guillaume-Gentil, O. et al. Tunable Single-cell extraction for molecular analyses. *Cell* **166**, 506-516 (2016).
25. Actis, P. Sampling from single cells. *Small Methods* **2**, 1700300 (2018).
26. Guillaume-Gentil, O. et al. Force-controlled manipulation of single cells: from AFM to FluidFM. *Trends Biotechnol*. **32**, 381-388 (2014).
27. Li, X., Tao, Y. L., Lee, D. H., Wickramasinghe, H. K. & Lee, A. P. In situ mRNA isolation from a microfluidic single-cell array using an external AFM nanoprobe. *Lab Chip* **17**, 1635-1644 (2017).
28. Seger, R. A. et al. Voltage controlled nano-injection system for single-cell surgery. *Nanoscale* **4**, 5843-5846 (2012).
29. Actis, P. et al. Compartmental genomics in living cells revealed by single-cell nanobiopsy. *ACS Nano* **8**, 546-553 (2014).
30. Tóth, E. N. et al. Single-cell nanobiopsy reveals compartmentalization of mRNA in neuronal cells. *J. Biol. Chem*. **293,** 4940-4951 (2018).
31. Kim, H., Okano, K., Osada, T., Ikai, A. & Yasuda, K. Development of mRNA analysis system in single living cells by atomic force microscopy. *Biophys. J.* **88**, 154A-154A (2005).
32. Osada, T., Uehara, H., Kim, H. & Ikai, A. Advances in Clinical Chemistry Vol 38 Ch. 3 (Elsevier, London, 2004).
33. Osada, T., Uehara, H., Kim, H. & Ikai, A. mRNA analysis of single living cells. *J. Nanobiotechnol*. **1:2**, (2003).
34. Nawarathna, D., Turan, T. & Wickramasinghe, H. K. Selective probing of mRNA expression levels within a living cell. *Appl. Phys. Lett*. **95**, 083117(2009).
35. Cadinu, P. et al. Single molecule trapping and sensing using dual nanopores separated by a zeptoliter nanobridge. *Nano Lett*. **17**, 6376-6384 (2017).
36. Cadinu, P. et al. Double barrel nanopores as a new tool for controlling single-molecule transport. *Nano Lett*. **18**, 2738-2745 (2018).
37. Takahashi, Y. et al. Multifunctional nanoprobes for nanoscale chemical imaging and Localized Chemical Delivery at Surfaces and Interfaces. *Angew. Chem., Int. Ed*. **50**, 9638-9642 (2011).
38. Ren, R. et al. Nanopore extended field-effect transistor for selective single-molecule biosensing. *Nat. Commun*. **8**, 586 (2017).

39. McKelvey, K. et al. Fabrication, characterization, and functionalization of dual carbon electrodes as probes for Scanning Electrochemical Microscopy (SECM). *Anal. Chem.* **85**, 7519-7526 (2013).
40. Freedman, K. J. et al. Nanopore sensing at ultra-low concentrations using single-molecule dielectrophoretic trapping. *Nat. Commun*. **7**, 10217(2016).
41. Ramos, A., Morgan. H., Green, N. G. & Castellanos, A. The role of electrohydrodynamic forces in the dielectrophoretic manipulation and separation of particles. *J Electrostat*, **47,** 71-81 (1999).
42. Barik, A. et al. Graphene-edge dielectrophoretic tweezers for trapping of biomolecules. *Nat. Commun***.** **8**, 1867 (2017).
43. Barik, A. et al. Ultralow-power electronic trapping of nanoparticles with sub-10 nm gold nanogap electrodes. *Nano Lett***.** **16**, 6317-6324 (2016).
44. Shivalingam, A. et al. The interactions between a small molecule and G-quadruplexes are visualized by fluorescence lifetime imaging microscopy. *Nat. Commun*. **6**, 8178 (2015).
45. Gibbons, J. G., Branco, A. T., Yu, S. & Lemos, B. Ribosomal DNA copy number is coupled with gene expression variation and mitochondrial abundance in humans. *Nat. Commun*. **5**, 4850 (2014).

Data Availability

The data that support the plots within this paper and other findings of this study are available from the corresponding author upon reasonable request

Additional Information

Supplementary information is available in the online version of the paper. Reprints and permission information is available online at www.nature.com/reprints. Correspondence and requests for materials should be addressed to J. B. E or A. I.

Acknowledgements

J.B.E. has been funded in part by an ERC starting (NanoP) and consolidator (NanoPD) investigator grant. A.I. acknowledges IC Research Fellowship funding. We acknowledge Bernice Akpinar for helping with the TEM and EDX spectroscopy. A.B. and S.-H.O. acknowledge support from the U.S. National Science Foundation (NSF ECCS #1610333).

Author Information

Contributions

J.B.E. and A.P.I., designed and supervised the research. B.P.N. and P.C. performed the experiments and contributed equally to this work. B.P.N., P.C., J.B.E. and A.P.I. analysed the data and prepared the manuscript. A. B. and S.-H.O. developed the finite element model and performed the theoretical calculations. A. J. A., M. J. D, J. G.-G., and B. W.-S. prepared the cell samples and contributed to the cell biopsy experiments. M. K. recorded the electron micrographs. J. T. K, K. R. W., R. V., and P. A helped with the experiments. All authors discussed the results and commented on the manuscript.

Competing interests

The authors declare no competing financial interests.

Supplementary Information

Supplementary Text, Supplementary Figures 1–14, Supplementary Table 1

Figure Captions

Fig. 1. Schematic and characterisation of the DEP nanotweezer. **a**, Application of an *AC voltage* on the nanotweezer generates a highly localised electric field gradient which is suitable for targeted molecular trapping in solution or inside a cell. **b,** SEM and TEM micrographs of the DEP nanotweezer before (i,ii) and after (iii, iv) carbon deposition (scale bars: i,iii 20 nm and ii,iv 100 nm), (n=10 independent micrographs). **c**, Linear sweep voltammograms recorded for each of the two electrodes for a typical nanotweezer using $(Ru(NH_3)_6)Cl_3$,

(n=5 independent measurements); inset shows the distribution of electrode radii calculated from the limiting currents (n= 17 independent measurements). **d**, (i) Electric field gradient distribution at the nanotweezer tip along the z-axis (x=y=0, f_A = 1 MHz, V_{pp} = 20 V) obtained from FEM model and (ii) plot of threshold electric field gradient required for trapping of double-stranded DNA. **e**, FEM model plot of temperature distribution around the nanotweezer tip in different ionic strengths along the z-axis (x=y=0).

Fig. 2. Trapping and extraction of 10 kbp DNA: **a**, The DEP force generated around the tip is sufficiently strong to capture freely diffusing DNA molecules in solution. This operation is fully reversible; as soon as the electric field is turned off the trapped molecules are immediately released back into the solution. Panels (**i**) to (**iv**) show fluorescence images recorded at the nanotweezer tip during trapping and releasing (f_A = 1 MHz, V_{pp} = 20 V) of YOYO-1 labelled 10 kbp DNA (100 pM 10 kbp DNA in 1 mM KCl, scale bar 5 µm). **b**, Fluorescence intensity-time trace of a typical DEP trapping experiment. **c**, Fluorescence intensity at the nanotweezer tip as a function of voltage (f_A = 1 MHz) and **d**, Frequency (V_{pp} = 20 V). All these results were verified independently by repeating the experiments using 4 different nanotweezers. **e**, Mean qPCR amplification curve for the extracted 10 kbp DNA along with positive (0.4 ng of 10 kbp DNA) and negative controls (DI water). Error bars indicate the standard deviation of 4 individual measurements.

Fig. 3. Nanotweezer aided single-molecule trapping and extraction. **a**, Fluorescence image showing YOYO-1 labelled 10 kbp DNA (highlighted with dashed circles) along with a bright field image displayed as an inset (scale bars 20 µm). **b**, and **c**, two different examples of trapping and release of individual DNA molecules (1 mM KCl solution, f_A = 2 MHz, V_{pp} = 10 V, scale bar 4 µm), (n=4 independent measurements). **d**, Three independent fluorescence-time trace showing single λ-DNA trapping events (V_{pp} = 10 V, f_A = 6 MHz). **e**, Amplification curves obtained from the qPCR of DEP-trapped λ-DNA molecules shown in **d.** Positive control is the mean of 4 individual measurements and the error bars indicates the standard deviation. **f**, Sequencing showing a near perfect match between the extracted DNA (Query) and aligned with the corresponding λ-DNA sequence (subject). **g, '***Pick-and-place'* of single molecules. (i) The DNA molecule was captured at the nanotweezer tip by turning on the AC field. (**ii**) and (**iii**), transfer of the captured single molecule from one position to another by moving the nanotweezer using a micromanipulator while the AC field was kept on. (**iv**), Release of the captured molecule by turning off the DEP (scale bars: i-iv 10 µm, insets 2 µm). Similar results were obtained while repeating these experiments (see Supplementary Information section 10)

Fig. 4. DNA extraction from the cell nucleus. **a.** Optical micrograph showing the nanotweezer inside the cell. Optical **b**, and fluorescent **c**, a micrograph of a typical HPAEC cell showing DNA in the nucleus (blue) and RNA (green). Scale bars 5 µm, (n=5 independent micrographs). Step-by-step schematics **d** and corresponding fluorescent images **e** of a single cell biopsy. **i)** The tip was approached and then inserted into the cell nucleus. **ii)** Application of an *AC* bias traps DNA fragments at the nanotweezers tip as can be seen by an increase in fluorescence signal around the tip. (**iii**) In the final step, the nanotweezer along with the accumulated material was withdrawn from the cell, and the presence of DNA was confirmed by the fluorescence spot localised at the very end of the tip (Scale bars: 10 µm, insets 2 µm), (n=4 independent measurements). **f** and **g**, Mean qPCR amplification curve and typical melting curves of the extracted DNA using 45S ribosomal DNA specific primers. Error bars indicate the standard deviation of 4 individual measurements.

Fig. 5. mRNA extraction from the cytoplasm. **a**, Targeted mRNA trapping and extraction was performed by labelling, via in situ hybridisation, of individual ETS-1 mRNA molecules with FITC (shown as green dots) (**i**). A high-resolution image of individual ETS-1 mRNA molecule (**ii**) along with a superimposed bright field image (inset). Application of the AC voltage results in trapping of the mRNA at the nanotweezers tip (**iii**) which was then pulled away by the subsequent withdrawal of nanotweezers causing a drop in the fluorescence signal (**iv**). Scale bars: i) 25 µm (inset: 5 µm); ii) 10 µm (inset: 2 µm); iii) & iv) 1 µm, (n=4 independent measurements). **b**, Biopsies were also performed in cells stained with a non-specific RNA dye (RNA Select®). The accumulation of labelled mRNA around the nanotweezers during DEP capture results in an increase in fluorescence at the

nanotweezers tip (**i-ii**). The mRNA can still be seen at the tip once extracted from the cell **(iii).** (scale bar: 20 µm and 5 µm for the insets), (n=4 independent measurements). **c,** and **d**, Mean qPCR amplification and melting curves obtained for *ACTB* cDNA synthesised from the extracted sample. Error bars indicate the standard deviation of 4 individual measurements.

Fig. 6. Single organelle extraction. **a**, Schematic of single mitochondrion extraction from the axon of mouse primary hippocampal neurons. **b**, Mitochondria were selectively stained using MitoTracker Green and optically visualised inside the neuron cells (scale bar 20 µm). **c**, The nanotweezers was positioned close to a labelled mitochondrion (**i**). Upon application of an *AC* field, the mitochondrion was attracted towards the tip (**ii**) and was subsequently removed from the neuron (**iii**) **d,** This process was confirmed by monitoring the variation in fluorescence signal at the extraction point, (n=4 independent measurements). **e**, Fluorescence of TMRM labelled mitochondrion in i) intact, ii) trapped and iii) extracted state were compared to confirm its viability before, during and after the manipulation. (scale bars 2 µm), (n=4 independent measurements).

Materials and Methods

Materials: Potassium chloride and Tris-EDTA, used for trapping experiments were purchased from Sigma-Aldrich. DAOTA-M2 used for DNA staining whereas SYTO™ RNA select® was used for RNA staining and purchased from Molecular Probes, Inc. These solutions were prepared fresh in Milli-Q water on the day of use. 10 kbp DNA and λ-DNA (both 500 µg/ml) were purchased from New England Biolabs, UK.

DNA labelling and fluorescence imaging: Labelled DNA samples (both 10 kbp and λ-DNA) for imaging was prepared by incubating 250 pM 10 kbp DNA solution in 10 mM Tris 1 mM EDTA with YOYO-1 (Molecular Probes) at a ratio of 1 YOYO-1 molecule per five base pairs. α-Synuclein (Sigma Aldrich) modified with Alexa 488 and diluted as needed. All fluorescence images and videos were acquired by using an optical microscope (IX71, Olympus) with a 60X water-immersion objective (1.20 NA, UPLSAPO 60XW, UIS2, Olympus) in conjunction with an electron multiplying CCD camera (Cascade II, Photometrics). Illuminating of the sample was performed with a fibre coupled 488 nm tuneable Argon Ion laser (Melles Griot, Model: 35-LAP-431-230).

Cell culture: Human bone osteosarcoma U2OS cells (obtained from London Research Institute, Cancer Research UK, authenticated and mycoplasma tested by the supplier) were grown in low glucose phenol red-free Dulbecco's modified Eagle medium containing 10% fetal bovine serum at 37 °C with 5% CO_2 in humidified air. Cells were seeded into an 8 well µ-slide (IBIDI) at a density of 20,000 cells/200 µl for 6–24 h before the experiments. Primary HPAEC, (obtained from Promocell, Germany, authenticated and mycoplasma tested by the supplier) were cultured at 37 °C, 5% CO_2 in EGM-2 media (Promocell) and used between passages 4-10. HPAEC were seeded into an 8 well µ-Slide (IBIDI) at a density of 20,000 cells/200 µl and left to incubate for 24 h. To visualise the extraction of DNA and RNA from the cells, the U2OS cells were first stained by using DAOTA-M2 and HPAEC using SYTO™ RNASelect™ dye respectively. For this, the media in the µ-Slide was replaced with fresh media containing the dye for the specified period and concentration (5–20 µM, 4–24 h, 200 µl). Before imaging, the cells were washed with PBS, and the incubation medium was replaced with fresh growth media. Primary hippocampal cultures were prepared as from E16 mice. Following a 15 min treatment with 0.25% trypsin and trituration, cells were seeded on poly-L-lysine coated, round, 12-mm coverslips or 8 well µ-Slide (IBIDI) at a density of 25,000 cells/cm^2. The cells were then incubated at 37 °C with 5% CO2 for 6-7 days. Neurons were loaded with 20 nM TMRM (Life Technologies) for 30 min at 37 °C or with 200 nM MitoTracker Green FM (Thermo Fisher) for 20 min at 37 °C. Before imaging, the cells were washed with PBS, and the incubation medium was replaced with conditioned growth media.

Single-cell biopsies: The nanotweezer was mounted on a micromanipulator (PatchStar, Scientifica) perpendicular to a chambered coverglass containing the cells placed on an optical microscope (IX71, Olympus) stage. The microscope was, in turn, mounted on a vibration isolation table (PTM51509, Thorlabs). To visualise the extraction of DNA, RNA or mitochondria from live, fluorescently labelled cells, the chambered coverglass containing stained cells was then mounted on the microscope stage. The nanotweezer was then inserted into the cell for the desired time (10-30 s), and extraction was initiated by turning on the electric field gradient which was visualised by using fluorescence microscopy as an increase in fluorescence around the nanotweezer tip. Upon completion of the procedure, the nanotweezer tip was retracted from the cell while holding the *AC*

voltage. The presence of a fluorescence spot at the tip after retraction confirmed the successful extraction of target molecules. Switching off the *AC* voltage across the nanotweezer electrodes turns off the electric field gradient leading to the release of DNA/RNA molecules from the nanotweezer tip. Control experiments, where the nanotweezer was inserted into the cells, but no *AC* field was applied, yielded no measurable increase of fluorescent intensity at the tip, confirming that molecules were extracted due to DEP trapping, rather than nonspecific adsorption to the nanoscale tip.

For the extraction of DNA and RNA for further analysis, a slightly different protocol was adopted. Briefly, the nanotweezer was approached towards the cell using the micromanipulator. The position of the nanotweezer was monitored using light microscopy. Once the nanotweezer was inserted into the cell, a field was generated at the nanotweezer tip by applying an *AC* voltage between the electrodes using a standard function generator (TG2000, TTi UK). The electric field gradient thus traps and concentrates the DNA/RNA molecules around the nanotweezer. After holding the nanotweezers tip inside the cell for a desired time (10-30 s), the tip was slowly retracted from the cell into the air through the growth media while keeping the *AC* voltage on. Once the nanotweezer tip was in the air, the *AC* field was switched off to complete the extraction. The extracted DNA/RNA on the nanotweezer tip was then transferred into the qPCR tube for further analysis by inserting the nanotweezer to the tube containing 5 µl of 10 mM Tris HCl (pH 8.5) and breaking the very end of the nanotweezer inside the solution.

RNAscope® in-situ hybridisation and immunostaining: For fluorescent in situ hybridisation, cells were processed using RNAscope® Multiplex Fluorescent Reagent Kit v2 (Advanced Cell Diagnostics) and TSA Fluorescein System (PerkinElmer), according to the manufacturer's protocol. Hybridisation was carried out with target probes (Hs-ETS1-C1, NM_001143820.1.

Cell viability test: The viability of cells after the biopsy procedure was confirmed by employing the trypan blue staining method. For this, the cell that underwent the biopsy was incubated for 3 min at room temperature with an equal volume of 0.4% (w/v) trypan blue solution prepared in 0.81% NaCl and 0.06% (w/v) dibasic potassium phosphate. After incubation, the unbound dye solution was removed by gently washing with fresh growth media while visualising the cell using an optical microscope (IX71, Olympus) with a 60X water-immersion objective (1.20 NA, UPLSAPO 60XW, UIS2, Olympus) in conjunction with an electron multiplying CCD camera (Cascade II, Photometrics) interfaced with Micromanager 2.0.

Reverse Transcription of the extracted RNA: Reverse transcription (cDNA synthesis) of the extracted RNA was performed using a PCR machine (Techne TC-3000, Bibby Scientific) in an optical qPCR tube (Agilent Technologies). The RNA trapped at the nanotweezer tip was first transferred into the qPCR tube by inserting the nanotweezer into the tube containing 5 µl of nuclease-free water and breaking the very end of the nanotweezer inside the solution. To this 5 µL of the reaction mix (4 µL of 5x iScript reaction mix and 1 µL of iScript reverse transcriptase, both from iScript cDNA Synthesis Kit, Bio-RAD) was added. Following initial priming at 25 °C for 5 min, reverse transcription was performed at 46 °C for 20 min. This was followed by the reverse transcriptase inactivation at 95 °C for 1 min.

qPCR: All qPCR amplification experiments were carried out using a Stratagene Mx3005P qPCR (Agilent Technologies) in an optical qPCR tube (Agilent Technologies). The qPCR primer pairs used for the amplification were either obtained commercially or designed using Primer3 online software (http://bioinfo.ut.ee/primer3-0.4.0/) and Primer-BLAST (https://www.ncbi.nlm.nih.gov/tools/primer-blast/) and were obtained from Applied Biosystems UK (for a list of primers used in this study, see Supplementary Information section 15). The DNA trapped at the nanotweezer tip was first transferred into the qPCR tube by inserting the nanotweezer into the tube containing 5 µl of 10 mM Tris HCl (pH 8.5) and breaking the very end of the nanotweezer inside the solution. To this 10 µL of the qPCR master mix (iTaq™ Universal SYBR® Green Supermix, BIO-RAD), 1 µL each of the forward and reverse primers were added. The total volume was made up to 20 µL using nuclease-free water. Following an initial denaturation cycle of 95 °C for 5 min, 50 PCR cycles were performed (denaturation at 95 °C for 15 s, annealing/extension at 60 °C for 60 s). Fluorescence data were recorded at the end of each annealing/extension step. Melting peak analysis was performed by increasing the temperature at a rate of 0.5 °C/s from 60 to 90 °C, to confirm the validity of PCR.

DNA Sequencing: A segment of the extracted λ-DNA was first amplified using qPCR. The qPCR products were purified by using PureLink™ PCR Micro Kit (Invitrogen). The purified samples were then sequenced using the

569 Applied Biosystems Dye-Terminator Kit and analysed on an Applied Biosystems 3730 DNA analyser (Applied
570 Biosystems, CA). The sequence analysis was then carried out using BLAST (https://blast.ncbi.nlm.nih.gov).

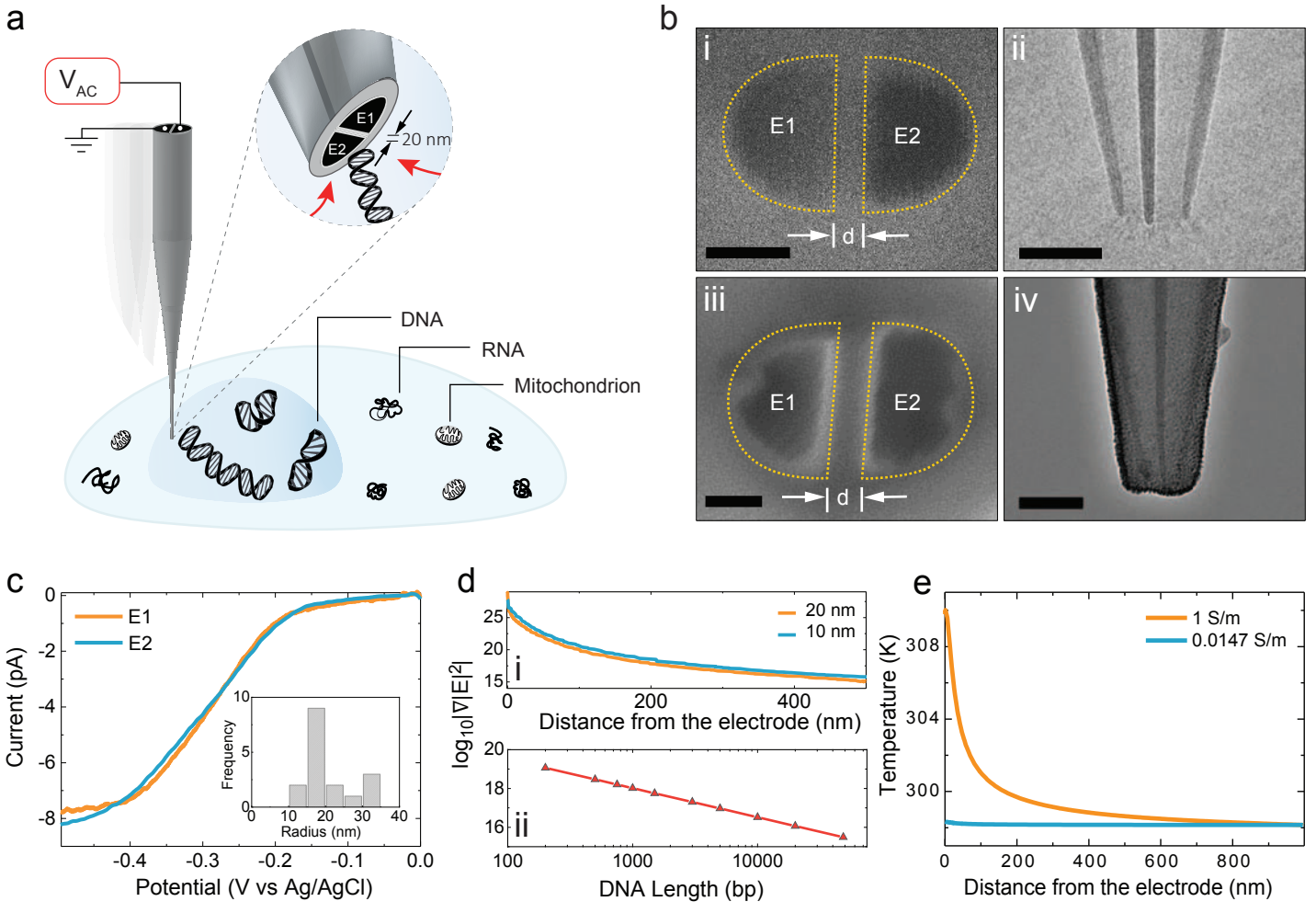
a
V_AC
E1
E2
20 nm
DNA
RNA
Mitochondrion
b
i
E1
E2
d
ii
iii
E1
E2
d
iv
c
E1
E2
Current (pA)
Potential (V vs Ag/AgCl)
Frequency
Radius (nm)
d
20 nm
10 nm
i
Distance from the electrode (nm)
log10|∇|E|2|
ii
DNA Length (bp)
e
1 S/m
0.0147 S/m
Temperature (K)
Distance from the electrode (nm)

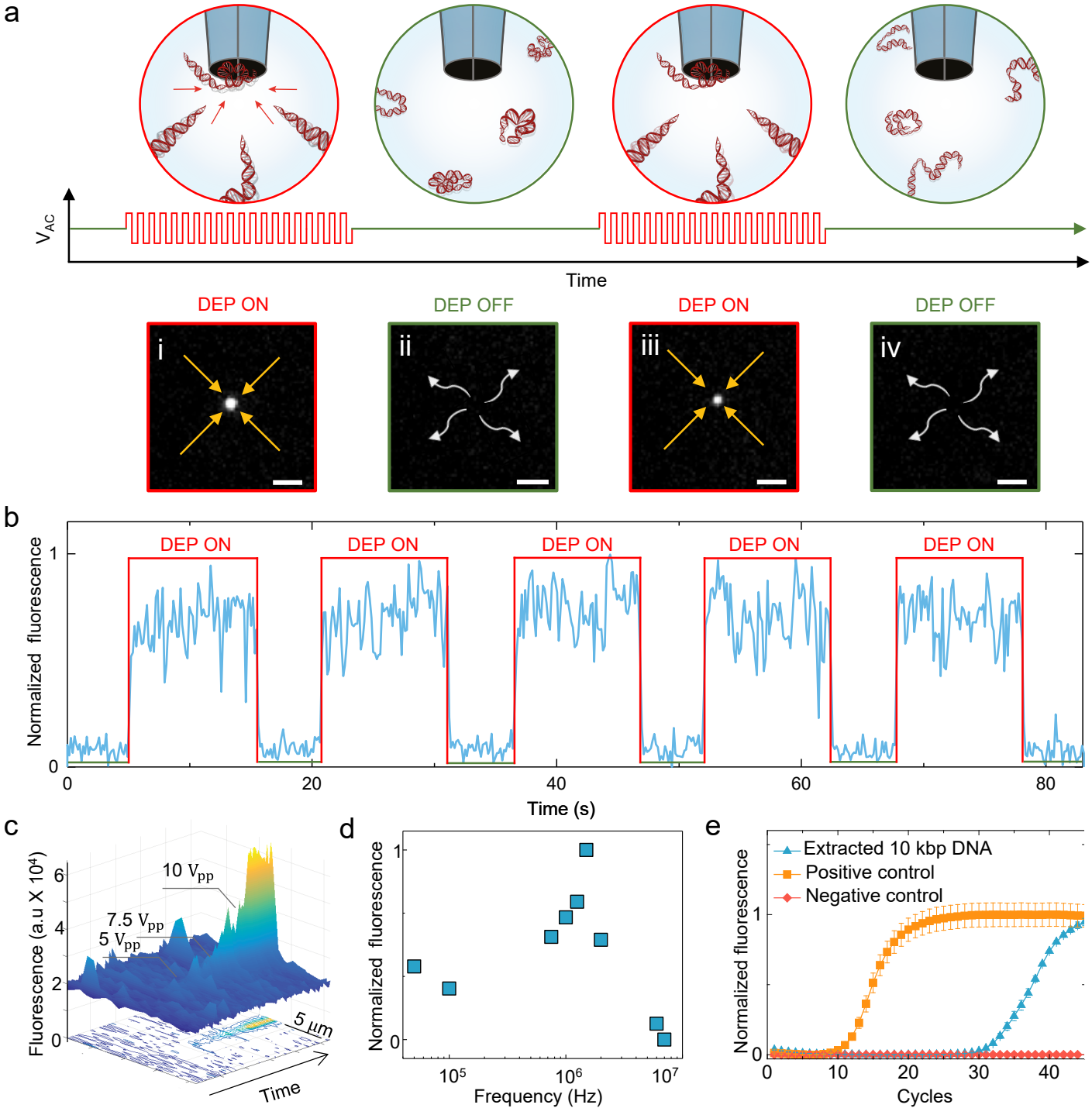
a
V_{AC}
Time
DEP ON
DEP OFF
DEP ON
DEP OFF
i
ii
iii
iv
b
Normalized fluorescence
DEP ON
DEP ON
DEP ON
DEP ON
DEP ON
Time (s)
c
Fluorescence (a.u X 10^4)
10 V_{pp}
7.5 V_{pp}
5 V_{pp}
5 µm
Time
d
Normalized fluorescence
Frequency (Hz)
e
Extracted 10 kbp DNA
Positive control
Negative control
Normalized fluorescence
Cycles

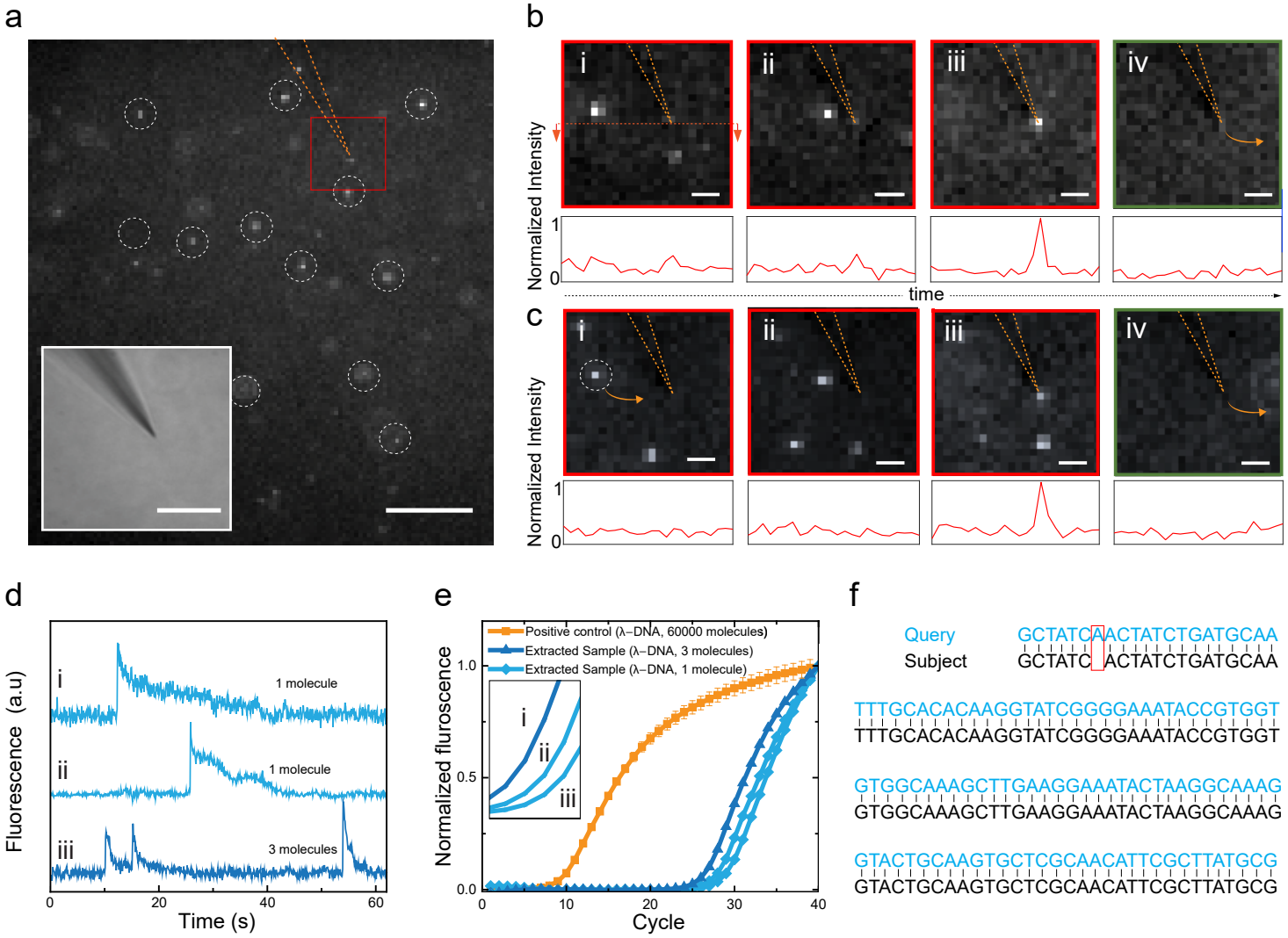
a
b
i
ii
iii
iv
Normalized Intensity
1
0
time
c
i
ii
iii
iv
Normalized Intensity
1
0
d
Fluorescence (a.u)
i
1 molecule
ii
1 molecule
iii
3 molecules
0
20
40
60
Time (s)
e
Positive control (λ−DNA, 60000 molecules)
Extracted Sample (λ−DNA, 3 molecules)
Extracted Sample (λ−DNA, 1 molecule)
Normalized fluroscence
1.0
0.5
0.0
i
ii
iii
0
10
20
30
40
Cycle
f
Query GCTATCAACTATCTGATGCAA
Subject GCTATC ACTATCTGATGCAA
TTTGCACACAAGGTATCGGGGAAATACCGTGGT
TTTGCACACAAGGTATCGGGGAAATACCGTGGT
GTGGCAAAGCTTGAAGGAAATACTAAGGCAAAG
GTGGCAAAGCTTGAAGGAAATACTAAGGCAAAG
GTACTGCAAGTGCTCGCAACATTCGCTTATGCG
GTACTGCAAGTGCTCGCAACATTCGCTTATGCG
g
Capture: DEP ON
Transfer: DEP ON
Transfer: DEP ON
Release: DEP OFF
i
ii
iii
iv

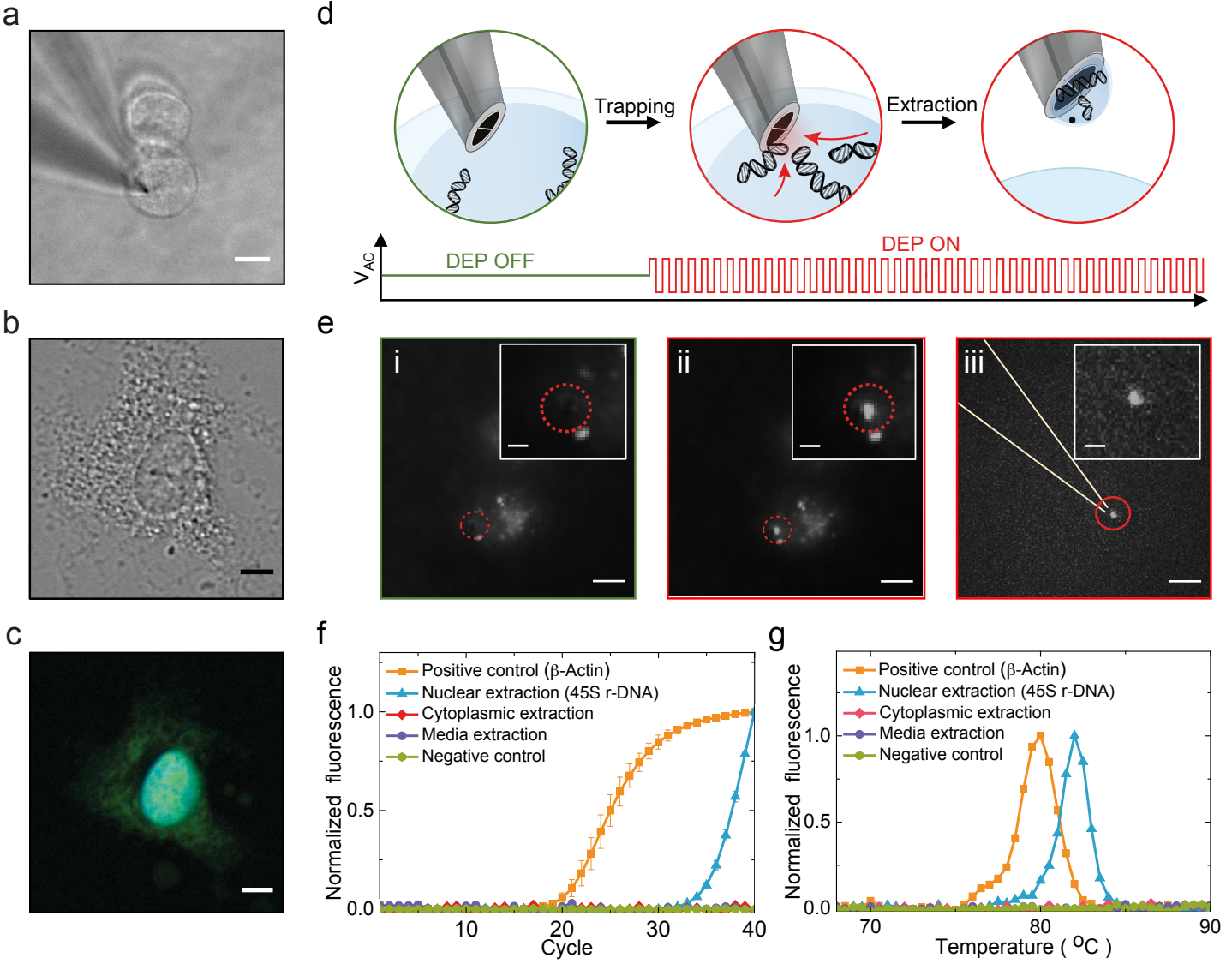
a
b
c
d
Trapping
Extraction
DEP OFF
DEP ON
V_{AC}
e
i
ii
iii
f
Positive control (β-Actin)
Nuclear extraction (45S r-DNA)
Cytoplasmic extraction
Media extraction
Negative control
Normalized fluorescence
Cycle
g
Temperature (°C)

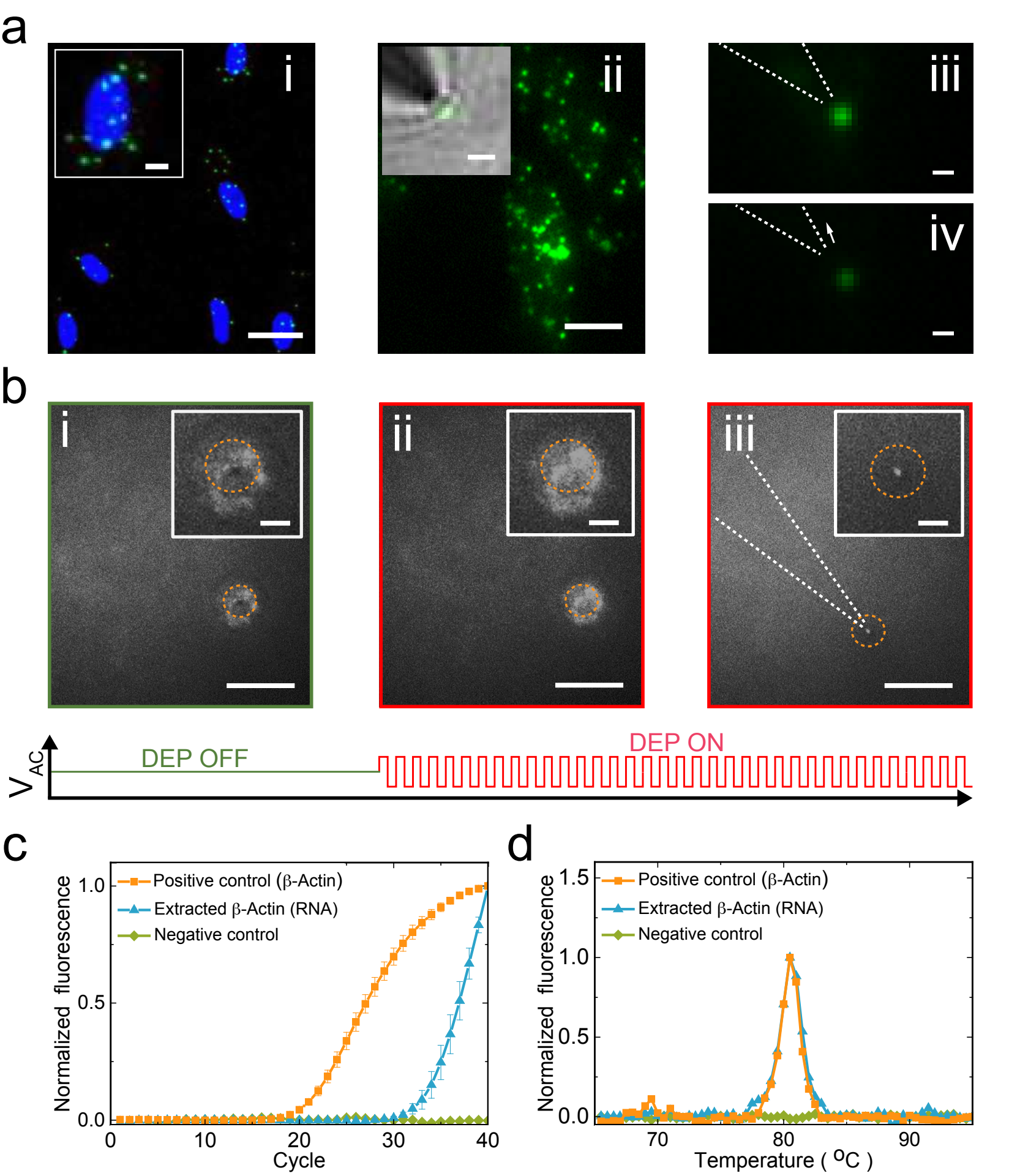
a
i
ii
iii
iv
b
i
ii
iii
DEP OFF
DEP ON
V_{AC}
c
Positive control (β-Actin)
Extracted β-Actin (RNA)
Negative control
Normalized fluorescence
Cycle
0.0
0.5
1.0
0
10
20
30
40
d
Positive control (β-Actin)
Extracted β-Actin (RNA)
Negative control
Normalized fluorescence
Temperature (°C)
0.0
0.5
1.0
1.5
70
80
90

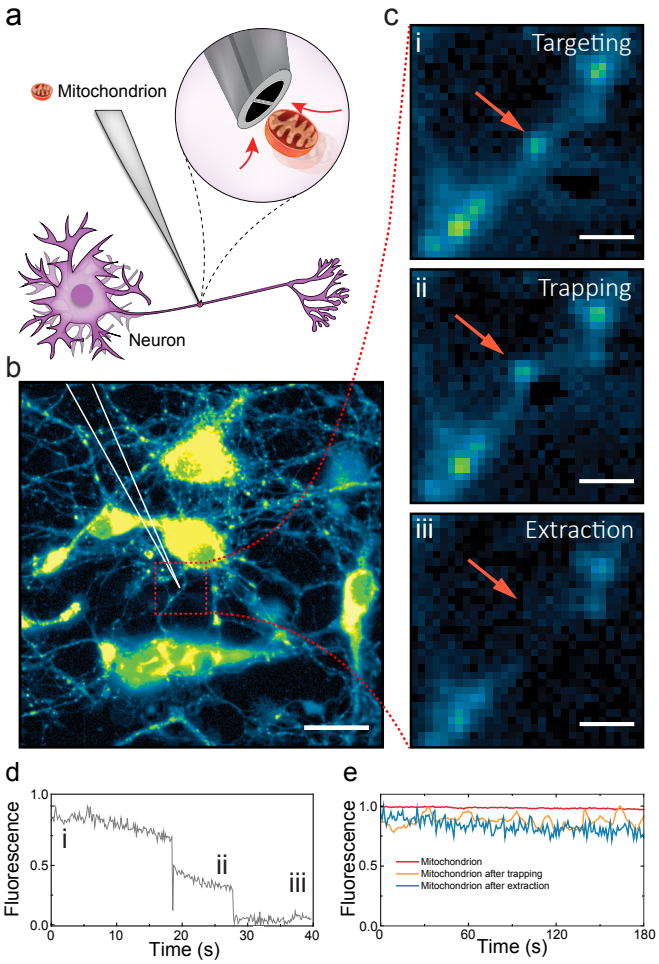
a
Mitochondrion
Neuron
b
c
i
Targeting
ii
Trapping
iii
Extraction
d
Fluorescence
Time (s)
i
ii
iii
e
Fluorescence
Time (s)
Mitochondrion
Mitochondrion after trapping
Mitochondrion after extraction